The Astrophysical Journal Letters, 730:L15 (5pp), 2011 April 1 doi:10.1088/2041-8205/730/2/L15

A STATISTICAL MODEL FOR THE γ-RAY VARIABILITY OF THE CRAB NEBULA

Qiang Yuan[1,2], Peng-Fei Yin[1], Xue-Feng Wu[2,3,4], Xiao-Jun Bi[1], Siming Liu[3], and Bing Zhang[2]
[1] Key Laboratory of Particle Astrophysics, Institute of High Energy Physics, Chinese Academy of Sciences, Beijing 100049, China
[2] Department of Physics and Astronomy, University of Nevada Las Vegas, Las Vegas, NV 89154, USA
[3] Purple Mountain Observatory, Chinese Academy of Sciences, Nanjing 210008, China
[4] Joint Center for Particle Nuclear Physics & Cosmology (J-CPNPC), Nanjing 210093, China
Received 2010 December 6; accepted 2011 February 14; published 2011 March 3

ABSTRACT

A statistical scenario is proposed to explain the γ-ray variability and flares of the Crab Nebula, which were observed recently by the *Fermi*/LAT. In this scenario electrons are accelerated in a series of knots, whose sizes follow a power-law distribution. These knots presumably move outward from the pulsar and have a distribution in the Doppler boost factor. The maximal electron energy is assumed to be proportional to the size of the knot. Fluctuations at the highest energy end of the overall electron distribution will result in variable γ-ray emission via the synchrotron process in the $\sim$100 MeV range. Since highly boosted larger knots are rarer than smaller knots, the model predicts that the variability of the synchrotron emission increases with the photon energy. We realize such a scenario with a Monte Carlo simulation and find that the model can reproduce both the two γ-ray flares over a period of $\sim$1 year and the monthly scale γ-ray flux fluctuations as observed by the *Fermi*/LAT. The observed γ-ray spectra in both the steady and flaring states are also well reproduced.

Key words: gamma rays: general – ISM: individual objects (Crab) – radiation mechanisms: non-thermal

Online-only material: color figures

1. INTRODUCTION

The Crab pulsar wind nebula is powered by its central pulsar born from a supernova explosion in 1054. It is a very luminous source in almost all wavelengths, from radio to the very high energy (VHE) γ-ray bands. The broadband non-thermal emission spectrum is well modeled by a synchrotron inverse Compton (IC) scenario (Atoyan & Aharonian 1996; Meyer et al. 2010) with the transition from the synchrotron to IC component occurring at a few hundred MeV (Abdo et al. 2010). The overall emission seems to be steady, so that the Crab Nebula has been adopted as a standard candle in high-energy astrophysics to calibrate observations from different instruments.

However, detailed images of the Crab Nebula in optical and X-ray bands indicated dynamical structures at small scales. Observations by the *Hubble Space Telescope* revealed wisps and knots in the nebula, and resolved some substructures of the highly variable wisps (Hester et al. 1995). X-ray observations by *ROSAT* and *Chandra* uncovered a jet–torus structure of the inner nebula (Hester et al. 1995; Weisskopf et al. 2000), and the equatorial ring is found moving outward with a speed of $\sim 0.5c$ (Hester et al. 2002). At higher energies in the γ-ray band, detailed structures of the nebula generally cannot be resolved. However, COMPTEL and EGRET observations indicated that the synchrotron radiation in 1–150 MeV is variable on a timescale of $\sim$1 yr (Much et al. 1995; de Jager et al. 1996).

In 2010 September, *AGILE* collaboration reported a γ-ray flare above 100 MeV from the direction of the Crab Nebula, which lasted for about 3 days (Tavani et al. 2010, 2011). The flux during the flare period is about 2–3 times higher than the average flux. This flare was soon confirmed by the *Fermi*/LAT collaboration (Buehler et al. 2010), and an archive search of the *Fermi*/LAT data revealed another flare in 2009 February (Abdo et al. 2011). There were many other simultaneous or follow-up measurements for the flare in 2010 September in X-ray, optical, infrared, and radio bands. However, no significant flux enhancement was discovered. In the VHE γ-ray energies, ARGO–YBJ collaboration claimed the detection of a flux enhancement around TeV, with a possibly longer duration (Aielli et al. 2010). However, MAGIC and VERITAS observed the source with a shorter duration during the flare phase and did not reveal any enhancement in flux (Mariotti 2010; Ong 2010).

It was proposed that the flares were due to synchrotron emission of ultra-relativistic electrons with energies up to $\sim$PeV (Abdo et al. 2011). Considering the fact that the rest-frame synchrotron radiation in a magnetic-field-dominated acceleration regime cannot exceed $\sim$70 MeV due to the fast synchrotron cooling of high-energy electrons (Blumenthal & Gould 1970; Lyutikov 2010), the observed GeV emission implies Doppler shift of the radiation region or other acceleration mechanisms instead of shock acceleration (Abdo et al. 2011). Komissarov & Lyutikov (2010) proposed that the γ-ray variability (flare) originated from the "inner knot" of the Crab Nebula ("knot 1" as defined in Hester et al. 1995), with mildly Doppler-boosted emission. The instability of the termination shock may cause the variability as revealed by magnetohydrodynamic (MHD) simulations. Bednarek & Idec (2010) suggested that electrons are accelerated in a region behind the shock, and the variability was attributed to changes in the maximum energy of accelerated electrons, electron spectral index, or the magnetic field.

In this Letter, we employ a statistical approach to model the γ-ray variability of the nebula. *Fermi*/LAT observations have shown that the low-energy synchrotron component is variable on a monthly timescale, while the high-energy IC component seems to be stable (Abdo et al. 2011). Since the synchrotron γ-rays are produced by the highest energy electrons, these observations indicate that fluctuations at the high-energy end of the electron distribution might be responsible for the variability. It is natural to expect that events that can generate the highest energy electrons are rarer, and therefore would lead to the largest fluctuation. Therefore, the variability

and flares in the sub-GeV γ-rays can be simply due to the statistical fluctuation of the highest energy electrons achievable in the electron accelerators. Lower energy electrons do not suffer from significant fluctuations since many more accelerators can contribute to them simultaneously, which gives rise to a "steady-state" emission in both the lower energy synchrotron component and the higher energy IC component.

2. THE MODEL AND RESULTS

We build a physically possible model to investigate the above picture in more detail. We assume that electrons are accelerated in a series of knots with a power-law energy spectrum $F_i(E) \propto E^{-\alpha_e}$ with the maximum electron energy $E^i_{\rm max}$ being proportional to the size of the ith knot.[5] We further assume that the size of knots has a power-law distribution $P(r_i) \propto r_i^{-\beta}$. Adding the contribution from all these knots together, noticing that the normalization of the synchrotron spectrum of the knots scales as r_i^3, we get the total electron spectrum as

$$\begin{aligned} F(E) &\propto \int F_i(E)\Theta\left(E^i_{\rm max} - E\right) \times r_i^3 P(r_i) dr_i \\ &\propto \int E^{-\alpha_e}\Theta\left(E^i_{\rm max} - E\right) \times {E^i_{\rm max}}^{3-\beta} dE^i_{\rm max} \\ &= E^{-\alpha_e} \int_E^{E_{\rm max}} {E^i_{\rm max}}^{3-\beta} dE^i_{\rm max}, \end{aligned} \quad (1)$$

where $\Theta(x)$ is the Heaviside step function and $E_{\rm max}$ is the maximum energy of the largest knot. If $\beta > 4$, the above integral of the last step is approximately proportional to $E^{4-\beta}$ given the maximum energy of the largest knot $E_{\rm max} \gg E$; if $\beta < 4$, the integral is nearly a constant determined by $E_{\rm max}$. Therefore, the electron spectrum is a power law $F(E) \propto E^{-\alpha}$ with power-law index $\alpha = \max(\alpha_e + \beta - 4, \alpha_e)$ and a cutoff determined by the largest knot.

The maximal energy of synchrotron emission in the magnetic-field-dominated acceleration regime is $\sim$70 MeV (Blumenthal & Gould 1970; defined by equating the synchrotron cooling timescale to the gyroperiod, the minimum of the acceleration timescale). For smaller accelerators, the maximum energy is also limited by the size of the accelerator. In order to account for the observations in the $\sim$100 MeV range, we therefore further employ a mild Doppler boost factor. We assume a Gaussian distributed Lorentz factor of all the knots with a mean value $\Gamma = 2.0$ and a standard deviation $\sigma = 0.25$. Such a Lorentz factor is consistent with the upper limit of the typical velocity of the jet (Abdo et al. 2011). We assume that the angle θ between the knot motion and the line of sight is randomly distributed. The Doppler factor $\delta = 1/\Gamma(1 - v\cos\theta)$ (where v is the velocity of the knot in unit of c) therefore is distributed within the range 0.18–5.5 for a 3σ distribution of Γ. Only knots with large enough size and large enough Doppler factor can contribute to high-energy synchrotron radiation to account for the flares observed by the *Fermi*/LAT.

We realize such a picture by a Monte Carlo simulation. We directly simulate the synchrotron spectrum in each knot instead of the electron spectrum. The synchrotron spectrum of each knot in its comoving frame is adopted as $\nu' F_{\nu'} \propto \nu'^{-\alpha_\nu} \exp(-\nu'/\nu'_{\rm max})$, where $\nu'_{\rm max} \propto (E^i_{\rm max})^2 \propto r_i^2$ and $\alpha_\nu = (\alpha - 3)/2$ is the synchrotron spectral index, with α being the power-law index of the overall electron distribution. The magnetic field in each knot is not explicitly used in the calculation. The magnetic field will affect the cooling break of the low-energy synchrotron spectrum as well as the high-energy cooling timescale. To keep the basic framework of the present study, we may expect the magnetic field to not vary significantly with respect to the knot size.

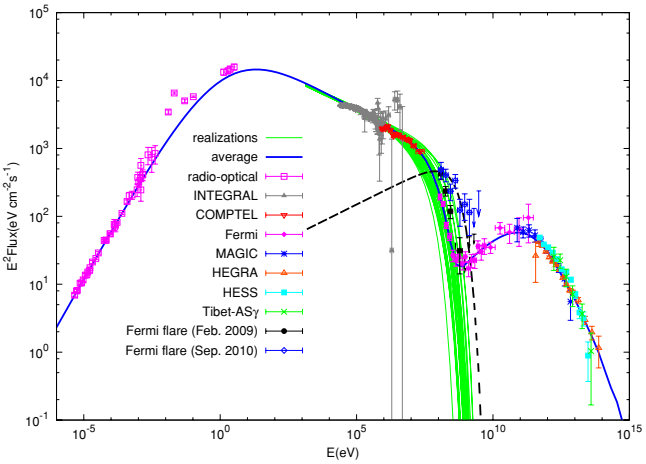

Figure 1. Spectral energy distribution of the Crab Nebula. The thin green lines denote the simulated synchrotron spectra of 30 realizations. The thick blue line denotes the fit to the multi-wavelength steady-state observational data, which can be understood as the average result of many realizations in our model. The black-dashed curve denotes the contribution from a maximum size knot with slightly specific parameters (see the text), which is shown to be able to explain the large flare in 2010 September. The references of the observational data are: radio–optical (Macías-Pérez et al. 2010), *INTEGRAL* (Jourdain & Roques 2009), COMPTEL (Kuiper et al. 2001), *Fermi*/LAT (Abdo et al. 2010), MAGIC (Albert et al. 2008), HEGRA (Aharonian et al. 2004), HESS (Aharonian et al. 2006), Tibet-ASγ (Amenomori et al. 2009), and *Fermi*/LAT flares (Abdo et al. 2011).

(A color version of this figure is available in the online journal.)

The energy loss of electrons in the knots can be important and needs to be considered. For instantaneous injection of accelerated electrons, the probability of observing electrons at a given energy is proportional to the corresponding synchrotron cooling time $t_c \propto E^{-1}$. For low-energy electrons with cooling time longer than the age of the Crab Nebula $t_{\rm age} \approx 10^3$ yr, these electrons will survive and accumulate. Therefore, we can construct a probability function $P(E) = 1/(1 + t_{\rm age}/t_c)$, describing the effect of cooling on the electron spectrum. The cooling time of electrons producing synchrotron photon with energy ϵ is $t_c \simeq 1.5(B/{\rm mG})^{-1.5}(\epsilon/{\rm keV})^{-0.5}\delta^{-0.5}$ yr. For an average magnetic field $B \approx 0.1$ mG, a mildly Doppler factor $\delta \sim 1$, electrons producing photons with an energy $\epsilon \sim 2.5$ eV have a cooling time comparable to $t_{\rm age}$. The observed spectrum of Crab Nebula has a break near 2.5 eV (see Figure 1).

In this work we mainly focus on the high-energy part of the spectra, e.g., from X-ray to γ-ray band, then $P(E) \propto E^{-1}$. Assuming that the accelerated electrons have a spectrum index $\alpha_e^{\rm inj}$, the electron spectrum index in the synchrotron-cooling-dominated regime is then $\alpha_e = \alpha_e^{\rm inj} + 1$. Here we adopt $\alpha_e = 2.6$ which corresponds to $\alpha_e^{\rm inj} = 1.6$, as required by fitting the radio–optical data (Meyer et al. 2010). The maximum value of $\nu'_{\rm max}$ is taken as 55 MeV in the comoving frame (corresponding

[5] The maximum energy of electrons will reach a critical value when the synchrotron cooling is essential. The critical Larmor radius is estimated as $R_L^c \approx \sqrt{\frac{6\pi e}{\sigma_T B}\frac{m_e c^2}{eB}} \simeq 2\times10^{-3}(B/{\rm mG})^{-1.5}$ pc, which just corresponds to the size of the emission region as indicated by the day-scale flare. Therefore, we assume that the largest size of the knots is R_L^c, and for all other knots smaller than R_L^c the scaling relation between $E^i_{\rm max}$ and r_i can well hold.

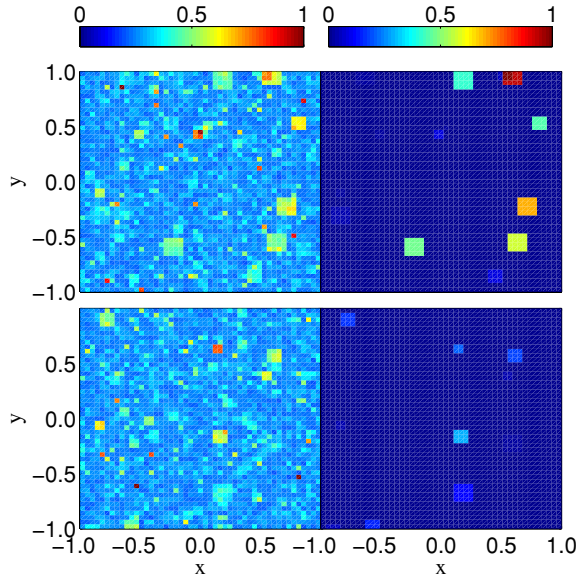

Figure 2. Upper and bottom panels represent two realizations of the synchrotron sky-maps at 10 keV (left) and 100 MeV (right) energies. The upper one shows a realization of a possible γ-ray flare, while the lower one shows a realization with relatively weak γ-ray emission.

(A color version of this figure is available in the online journal.)

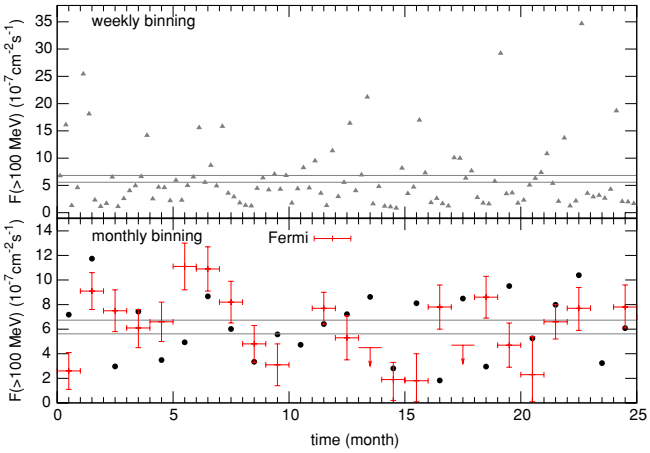

Figure 3. Light curves of the simulated synchrotron flux above 100 MeV. The upper panel shows the results with weekly bin and the bottom panel for monthly bin. The vertical axes in each panel indicate the average value of the simulations, which is normalized to the observational value $\sim 6.2 \times 10^{-7}$ cm^{-2} s^{-1} (Abdo et al. 2011). The *Fermi*/LAT observational data with monthly bin are also plotted in the lower panel.

(A color version of this figure is available in the online journal.)

to the largest knot). This value is derived according to a fit to the average *Fermi*/LAT spectrum of the synchrotron component (Abdo et al. 2010), given the Lorentz factor distribution. The power-law index of the size distribution is adopted as $\beta \approx 4.8$. Adding all the contribution from the knots together we can get a total synchrotron spectrum $\nu' F_{\nu'} \propto \nu'^{-0.2}$, which can reproduce the observed optical–MeV band data of the Crab Nebula (Figure 1). Note that these parameters, i.e., Γ, $\nu'_{\rm max}$, α_e, and β are not uniquely determined. What we adopt in this work is an illustration of the model. Once the data from optical to γ-ray band are reproduced, the discussion below is basically unchanged if a different set of parameters is taken.

For each knot we randomly generate an angle θ and a Lorentz factor Γ based on the assumed Gaussian distribution, and calculate the Doppler factor δ. Then the frequency of synchrotron emission from each knot is shifted from ν' to $\delta\nu'$, and the flux is enhanced to $\delta^3 F_{\nu'}$. The contribution from all the knots is summed up to obtain the total emission spectrum.

A series of simulated synchrotron spectra is shown in Figure 1, which are compared with the observational data of the Crab Nebula. Note that for the *INTEGRAL* data we adopt a flux normalization factor 0.6 in order to be consistent with the extrapolation of COMPTEL data. In Meyer et al. (2010), a 0.78 factor was adopted to match the *XMM-Newton* data. The difference of flux normalization may be due to discrepancies in calibration of different detectors. The fact that the *INTEGRAL* data may contain emission from the Crab pulsar may also contribute to the difference. For comparison we show the fitting results to the broadband data with the blue thick line, with a broken power-law electron spectrum. This result is similar to the model invoking two population electrons as introduced in Atoyan & Aharonian (1996) and Meyer et al. (2010). It is shown that the simulated synchrotron spectra have very small fluctuations in the X-ray energy band, but fluctuate significantly at higher energies (>1 MeV). The average of the simulated γ-ray flux would be consistent with the long-term *Fermi*/LAT and COMPTEL data. The fluctuations can be responsible for the observed variabilities and flares.

The very large flare at 2010 September that is not well reproduced by these simulations can be regarded as an event with very small probability. Such an event may be due to a large knot with specific parameters different from what used in the model. The black-dashed line in Figure 1 shows a possible reproduction of the large flare, produced by a knot with maximum size, Doppler factor $\delta = 5.5$, cutoff energy of synchrotron radiation in its comoving system 70 MeV, and an additional normalization factor 0.2 of the flux. Detailed modeling of the knot formation and its evolution is expected to better address this issue.

We pick out two realizations and show the synchrotron sky-maps at 10 keV (left) and 100 MeV (right) in Figure 2, respectively. To generate a sky-map, we designate an x–y plane with 50 × 50 pixels. We randomly assign a position for each knot in the x–y plane, with the largest knot having a size of 5 × 5 pixels. We then sum up contributions of all the knots located in each pixel and obtain the sky-map. It is shown that in the X-ray band (left panels) the sky-maps are relatively smooth with some hot spots due to several large knots. These hot spots may correspond to the *Chandra* and Hubble knots of the Crab Nebula (Tennant et al. 2010; Caraveo et al. 2010). The total flux of X-ray emission, however, is statistically steady from time to time. The width of the total X-ray flux distribution at ~10 keV is estimated to be of the order 1%, which is consistent with the upper limit of 5.5% obtained by *Swift*/BAT (Markwardt et al. 2010). The ~100 MeV γ-ray sky-maps could differ significantly from each other. In some cases, one or several large knots would dominate the total flux. The predicted energy-dependent spatial scales due to fluctuations may not be ready to test with the available high-energy telescopes, but higher angular resolution observations in the future will help.

According to our model, the IC component should not show significant variability except in the high-energy regime (>100 TeV), depending on the maximal electron energies. For example, for a magnetic field $B \approx 1$ mG, the maximal Lorentz factor of electrons can be as high as $\gamma_{\rm max} \sim \sqrt{6\pi e/\sigma_T B} \simeq 4\times10^9$. Therefore, only the IC photons with energies higher than several hundred TeV would have relatively large fluctuations.

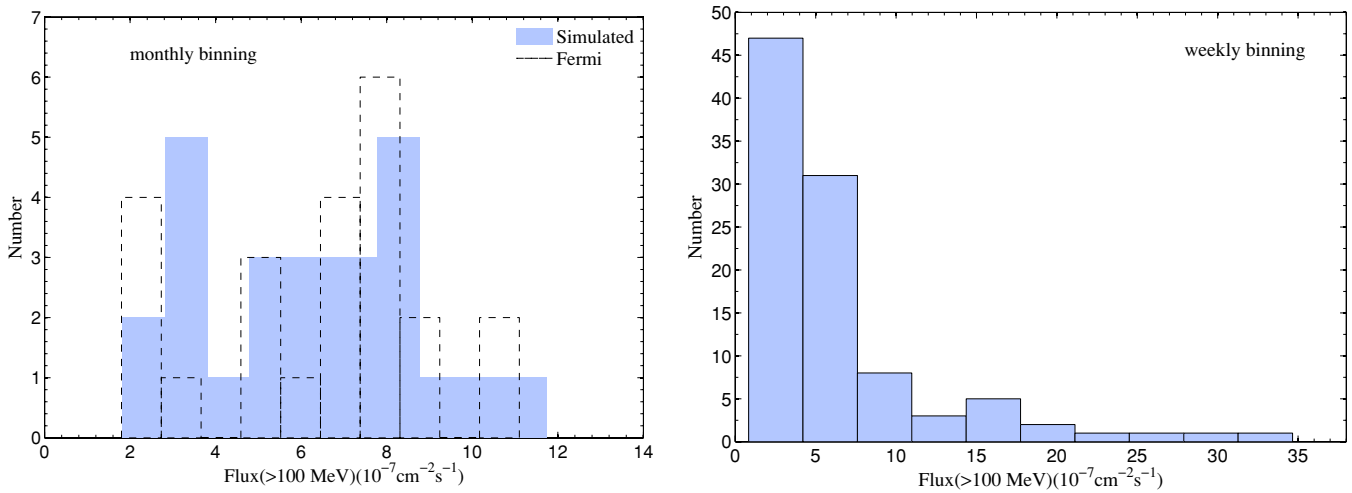

Figure 4. Histograms of the synchrotron flux distribution above 100 MeV, for monthly bin (left) and weekly bin (right), respectively. In the left panel, the *Fermi*/LAT observation result is also shown (dashed histogram).

(A color version of this figure is available in the online journal.)

This conclusion is different from that of Bednarek & Idec (2010), who suggested that the IC γ-ray spectra also vary significantly at multi-TeV energies.

To investigate fluctuations of emission in detail, we show in Figure 3 the light curves of the simulated synchrotron fluxes in the ∼100 MeV energy band. Each bin of the light curves represents an independent realization, and the length of the time bin is proportional to the number of knots. We normalize the timescale so that over a year there is an enhancement in flux by at least a factor of 5–6, which may be responsible for a flare, and plot the weekly and monthly bin light curves in the upper and lower panels of Figure 3, respectively. For comparison we also plot the *Fermi*/LAT observed monthly light curve (Abdo et al. 2011) in the lower panel of Figure 3. It can be seen that the predicted fluctuation level of the simulated results is very similar to that observed by *Fermi*/LAT. In order to show this more clearly, we plot the histogram of the monthly bin flux distribution for the simulated results along with that of *Fermi*/LAT observation in the left panel of Figure 4. These two distributions are indeed similar. In the right panel of Figure 4, the histogram of flux distribution for weekly bin is also plotted. A concentration toward low flux is evident, which is distinct from a symmetric distribution around the average value. This is because in the short timescale limit, the distribution of the γ-ray fluxes is determined by the distributions of the knots (power-law) and the Doppler factors. Only the knots with both large enough sizes and high enough Doppler factors can produce large γ-ray fluxes. Therefore, the probability to give large fluxes is very small, and the flux distribution concentrates toward low-flux values. In the limit of long timescale, the distribution should be Gaussian as a result of central limit theorem. Such a prediction can be tested by a detailed analysis of the *Fermi*/LAT data.

3. CONCLUSION AND DISCUSSION

In summary, we propose a statistical picture to explain the observed γ-ray variability and flares of the Crab Nebula, using the fluctuations of the highest end of the electron spectra. The electrons are thought to be accelerated in a series of knots, with a size distribution $P(r_i) \propto r_i^{-\beta}$ and a distribution of the Doppler factor. The maximal energy of the electrons in the comoving frame is assumed to be proportional to the size of the knots. Thus, the rare knots with large sizes and high Doppler boosts may generate electrons up to ∼PeV, and hence be responsible for the observed γ-rays flares at *Fermi*/LAT. On the other hand, the low-energy electrons are generated by many smaller knots. The average effect smooths the fluctuation, so that the low-energy synchrotron component and the IC component do not change significantly. This scenario can naturally explain both the variability in the MeV–GeV band, and the relatively steady emission in lower (optical, X-ray) and higher (TeV) energies. The expected variability of the monthly bin fluxes above 100 MeV is well consistent with that observed by *Fermi*/LAT. The two large γ-ray flares can also be naturally accounted for without additional assumptions.

In the simulation, we do not consider the detailed structure (e.g., jet, torus) of the nebula. The knots are assumed to have a uniform and isotropic distribution. Considering a more realistic morphology of the nebula would not affect our conclusion noticeably, as long as the distributions of the knot sizes and Doppler factors are similar to those introduced here. In more general terms, these knots may be interpreted as individual electron acceleration events distributed throughout the nebula. We point out that at low energies, contributions from large amount of knots are equivalent with previous studies that electrons are accelerated continuously inside the whole nebula. Although the model does not discuss the absolute timescales of flares and γ-ray fluctuations from the first principle, they may be related to timescales of developing MHD instabilities at different spatial scales.

We thank Zhuo Li, Shuang-Nan Zhang, Yi-Zhong Fan, Fang-Jun Lu, and You-Jun Lu for helpful discussions. This work is partially supported by the Natural Sciences Foundation of China grants 10773011, 11075169, 10633040, and 10921063, the 973 project grants 2010CB833000 and 2009CB824800, the NSF grant AST-0908362, and NASA grants NNX10AD48G and NNX10AP53G at UNLV.

REFERENCES

Abdo, A. A., et al. 2010, ApJ, 708, 1254
Abdo, A. A., et al. 2011, Science, 331, 739
Aharonian, F., et al. 2004, ApJ, 614, 897

Aharonian, F., et al. 2006, A&A, 457, 899
Aielli, G., et al. 2010, ATel, 2921
Albert, J., et al. 2008, ApJ, 674, 1037
Amenomori, M., et al. 2009, ApJ, 692, 61
Atoyan, A. M., & Aharonian, F. A. 1996, MNRAS, 278, 525
Bednarek, W., & Idec, W. 2010, arXiv:1011.4176
Blumenthal, G. R., & Gould, R. J. 1970, Rev. Mod. Phys., 42, 237
Buehler, R., D'Ammando, F., & Hays, E. 2010, ATel, 2861
Caraveo, P., et al. 2010, ATel, 2903
de Jager, O. C., Harding, A. K., Michelson, P. F., Nel, H. I., Nolan, P. L., Sreekumar, P., & Thompson, D. J. 1996, ApJ, 457, 253
Hester, J. J., et al. 1995, ApJ, 448, 240
Hester, J. J., et al. 2002, ApJ, 577, L49
Jourdain, E., & Roques, J. P. 2009, ApJ, 704, 17
Komissarov, S. S., & Lyutikov, M. 2010, arXiv:1011.1800
Kuiper, L., Hermsen, W., Cusumano, G., Diehl, R., Schönfelder, V., Strong, A., Bennett, K., & McConnell, M. L. 2001, A&A, 378, 918
Lyutikov, M. 2010, MNRAS, 405, 1809
Macías-Pérez, J. F., Mayet, F., Aumont, J., & Désert, F. 2010, ApJ, 711, 417
Mariotti, M. 2010, ATel, 2967
Markwardt, C. B., Barthelmy, S. D., & Baumgartner, W. H. 2010, ATel, 2858
Meyer, M., Horns, D., & Zechlin, H. 2010, A&A, 523, A2
Much, R., et al. 1995, A&A, 299, 435
Ong, R. A. 2010, ATel, 2968
Tavani, M., et al. 2010, ATel, 2855
Tavani, M., et al. 2011, Science, 331, 736
Tennant, A., et al. 2010, ATel, 2882
Weisskopf, M. C., et al. 2000, ApJ, 536, L81